THREE DIMENSIONAL HYPERSONIC FLOW SIMULATIONS WITH THE CSCM IMPLICIT UPWIND NAVIER-STOKES METHOD

87-1114

Jorge Bardina* and C.K. Lombard**

PEDA Corporation, Palo Alto, California 94303

Abstract

The computationally efficient three dimensional CSCM Navier-Stokes method of Bardina and Lombard has been extended to simulate complex external flows of hypersonic reentry vehicles at angle-of-attack. The stability and robustness of the shock capturing method has been improved with the addition of flux limiters and an inner approximation procedure in grid cells where changes of eigenvalue sign are present. The 3-D CSCM conservative-supra-characteristic method combines the best features of data management and computational efficiency of space marching procedures with the generality and stability of time dependent procedures to solve flows with mixed subsonic and supersonic zones, including streamwise separated flows. The robust stability of the method derives from the combination of conservative implicit upwind flux difference splitting, three-dimensional diagonally-dominant approximate factorization and relaxation scheme, and well-posed characteristic-based implicit boundary approximations. The efficiency of the method is based on an implicit symmetric Gauss-Seidel "method of planes" relaxation scheme with alternating directional space marching sweeps along the flow coordinate direction. A Newton-Raphson inner iteration procedure is employed with the implicit block-tridiagonal diagonally-dominant approximate factorization relaxation scheme for solution within the marching planes. This method requires less data in central memory and less total transfers of data into central memory per iteration than two data level linearized implicit schemes using only time-dependent approximate factorizations; therefore, the capability of processing larger and/or more complex data bases and computational grids is available. The efficiency of the 3-D CSCM algorithm makes this method very attractive to develop numerical procedures with equilibrium and nonequilibrium chemically reacting gases as is required for the simulation of hypersonic flows around vehicles flying at high altitudes.

Here this method is applied to simulate three dimensional hypersonic flows of a perfect gas around a sphere-cone-cylinder-flare reentry vehicle (RV) under angle of attack. The complex flow structures around the reentry vehicle under perfect gas conditions are well captured in a few hundred iterations. Results of the numerical simulation of the flow around the reentry vehicle under free stream angles of attack of 0° and 10° are presented, together with the results of the two-dimensional code for the simulation of the axisymmetric flow. Comparison shows excellent agreement between the two codes in the axisymmetric flow case.

*Staff Scientist, Member AIAA.

**President, Member AIAA.

Released to AIAA to publish in all forms.

Introduction

The effective engineering design of the new transatmospheric space vehicles flying at hypersonic speeds requires computational aerothermodynamics (CAT) technology in the frontier of present scientific research[1]. The aeroassisted orbital transfer vehicle (AOTV) to fly at Mach 30 in the upper atmosphere has the design requirement to predict the large low speed zone of recirculating flow with the turbulent wake behind this vehicle and represents a major research activity. Another major hypersonic vehicle under current investigation is the transatmospheric vehicle (TAV) which will fly into orbit from Earth's surface and land back using its own power. The design of these vehicles will require the integration of different areas of technology and research, in particular, the combination of an efficient three dimensional shock capturing CFD method such as the 3-D CSCM upwind method[2,3] with an efficient nonequilibrium chemistry procedure to account for the significant effects of thinner shock layer on drag and wall heat transfer due to high altitude flight and high temperatures that will be present.

The addition of chemical species conservation equations to the method[4] will impose severe challenges to stability due to different time and length scales of the chemistry, together with a large increase on data management and numerical processing in this kind of simulation. The 3-D CSCM method to be further described herein has resulted in a relaxation algorithm with efficient core storage requirements and substantially accelerated convergence over related two level linearized time dependent implicit methods. Accordingly the method provides a base where chemistry procedures can efficiently be exploited.

In its present form the algorithm is appropriate for transonic and supersonic aerodynamics and will shortly be presented in applications to equilibrium chemically reacting flow.

The 3-D CSCM method previously described in an application to internal flows by Bardina and Lombard[2] is an implicit "method of planes" symmetric Gauss-Seidel relaxation scheme. The data is conveniently stored on successive planes along the streamwise coordinate, and the system of equations is solved twice in each successive plane of the streamwise coordinate; along the forward direction, first, and along the backward direction, afterwards. In each plane the solution is obtained by a two level pseudo time dependent relaxation procedure based on the diagonally dominant approximate factorization DDADI[5]. The space marching alternating directional sweeps in the streamwise coordinate are von Neumann unconditionally stable[6,7] for zones of subsonic and streamwise separated and reversed flows as well as supersonic flow. Much as do the more restrictive PNS techniques, the present space marching method results in improved propagation of nonlinear effects to accelerate convergence to steady state. The method requires only a few 2-D cross-flow data planes in core at any

marching step and thus with fast disc storage, such as is available on the CRAY-XMP machines, can efficiently treat complex problems requiring very large numbers of mesh points in 3-D.

The purpose of the present paper is to describe important features of the 3-D CSCM method, and to show the performance of the method in the simulation of the hypersonic flowfield around a sphere-cone-cylinder-flare reentry vehicle (RV) at angle of attack. The code is substantially validated by comparison with results in axisymmetric flow for the generically similar 2-D/axisymmetric CSCM upwind code that has previously been extensively tested against experiment in both external and internal flows. For both classes of flows CSCM has demonstrated convective heat transfer capability[8].

In the following sections we will first describe the numerical method and then present the numerical results.

Conservative Difference Formulation

The conservative finite volume finite difference formulation of the 3-D compressible Navier-Stokes equations in general curvilinear coordinates $\xi(x,y,z)$, $\eta(x,y,z)$, and $\psi(x,y,z)$ is expressed, e.g. reference 9, as

$$\begin{aligned}\widetilde{J}\partial_t q+\bar{\bar{\xi}}_x\partial_\xi F+\bar{\bar{\xi}}_y\partial_\xi G+\bar{\bar{\xi}}_z\partial_\xi H+\\ \bar{\bar{\eta}}_x\partial_\eta F+\bar{\bar{\eta}}_y\partial_\eta G+\bar{\bar{\eta}}_z\partial_\eta H+\\ \bar{\bar{\psi}}_x\partial_\psi F+\bar{\bar{\psi}}_y\partial_\psi G+\bar{\bar{\psi}}_z\partial_\psi H=0\end{aligned} \tag{1}$$

where F, G, and H are the flux vectors in the Cartesian coordinate directions x, y, z, respectively; while q represents the conservative dependent variables,

$$q=(\rho\ ,\ \rho u\ ,\ \rho v\ ,\ \rho w\ ,\ e) \tag{2}$$

$$\begin{aligned}F=(\rho u\ ,\ \rho u^2+p-\sigma_{xx}\ ,\ \rho uv-\tau_{xy}\ ,\ \rho uw-\tau_{xz}\ ,\\ (e+p)u-u\sigma_{xx}-v\tau_{xy}-w\tau_{xz}-\kappa T_x)\end{aligned} \tag{3}$$

$$\begin{aligned}G=(\rho v\ ,\ \rho uv-\tau_{yx}\ ,\ \rho v^2+p-\sigma_{yy}\ ,\ \rho uw-\tau_{yz}\ ,\\ (e+p)v-u\tau_{yx}-v\sigma_{yy}-w\tau_{yz}-\kappa T_y)\end{aligned} \tag{4}$$

$$\begin{aligned}H=(\rho u\ ,\ \rho uw-\tau_{zx}\ ,\ \rho vw-\tau_{zy}\ ,\ \rho u^2+p-\sigma_{zz}\ ,\\ (e+p)w-u\tau_{zx}-v\tau_{yz}-w\sigma_{zz}-\kappa T_z)\ .\end{aligned} \tag{5}$$

Metric Coefficients

The metric coefficients of the generalized coordinate transformation are computed numerically as the interval averaged spatial difference formulas for the Cartesian coordinate grid points in the volume defined between the two adjacent grid points of the corresponding component of the flux difference vector, according to their mathematical definitions,

$$\begin{pmatrix}\bar{\bar{\xi}}_x & \bar{\bar{\xi}}_y & \bar{\bar{\xi}}_z\\ \bar{\bar{\eta}}_x & \bar{\bar{\eta}}_y & \bar{\bar{\eta}}_z\\ \bar{\bar{\psi}}_x & \bar{\bar{\psi}}_y & \bar{\bar{\psi}}_z\end{pmatrix}$$

$$=\begin{pmatrix}y_\eta z_\psi-z_\eta y_\psi & z_\eta x_\psi-x_\eta z_\psi & x_\eta y_\psi-y_\eta x_\psi\\ y_\psi z_\xi-z_\psi y_\xi & z_\psi x_\xi-x_\psi z_\xi & x_\psi y_\xi-y_\psi x_\xi\\ y_\xi z_\eta-z_\xi y_\eta & z_\xi x_\eta-x_\xi z_\eta & x_\xi y_\eta-y_\xi x_\eta\end{pmatrix} \tag{6}$$

The Jacobian of the transformation $\widetilde{J}$ is

$$\begin{aligned}\widetilde{J}=&x_\xi(y_\eta z_\psi-y_\psi z_\eta)+y_\xi(z_\eta x_\psi-x_\eta z_\psi)\\ &+z_\xi(x_\eta y_\psi-x_\psi y_\eta)\end{aligned} \tag{7}$$

Viscous Fluxes

The viscous terms of the flux vectors

$$\sigma_{xx}=2(\mu+\mu_\tau)(u_x-(u_x+v_y+w_z)/3)$$

$$\sigma_{yy}=2(\mu+\mu_\tau)(v_y-(u_x+v_y+w_z)/3)$$

$$\sigma_{zz}=2(\mu+\mu_\tau)(w_z-(u_x+v_y+w_z)/3)$$

$$\tau_{xy}=\tau_{yx}=(\mu+\mu_\tau)(u_y+v_x)$$

$$\tau_{yz}=\tau_{zy}=(\mu+\mu_\tau)(v_z+w_y)$$

$$\tau_{xz}=\tau_{zx}=(\mu+\mu_\tau)(u_z+w_x)$$

are second-order central differences in space and first-order implicit in time. These terms are treated in all but the ξ-streamwise coordinate direction with the Baldwin-Lomax[10] thin layer approximation.

When turbulence effects are present, they are modeled with the well known Baldwin and Lomax[10] mixing length model. This algebraic model defines an inner and outer layer formulation for the turbulent eddy viscosity in wall bounded shear layers, while only the outer layer is used for free shear layers and wakes. The main advantage of this model is that the velocity and length scales are easily defined and the model provides reasonable predictions. This model has been modified following the ideas of Bradshaw[11] for near wake flows, by setting a lower bound value for the wake law eddy viscosity as a function of the maximum viscosity value across the wake. This turbulence model has been used effectively to simulate axisymmetric wakes and jet-exhaust flows[12]. The flow of the present application around the forebody reentry vehicle at high altitude is essentially laminar. The turbulence model incorporated in the code would be useful in the simulation of the wake region or in aerodynamics problems at lower altitudes.

Inviscid Fluxes

The inviscid flux terms of equation (1) are approximated with CSCM flux difference eigenvector splitting in an extension of the approach of reference 5. First order upwind spatial differencing is unconditionally stable with backward Euler iteration. For higher order upwind spatial differences, we incorporate flux limiters for unconditionally linear stability from reference 13.

The CSCM-S method, which is a (globally) single data level relaxation technique, is employed in marching along the ξ-direction. Within a ξ constant plane at each marching step the implicit equations are relaxed using the pseudo time dependent CSCM method which is a two data level relaxation technique employed along ψ and η directions. planes. The resulting implicit method of planes with one (additional) inner iteration at each spatial (ξ) marching step provides a faster convergence of the solution for nonlinear systems of equations. While the processing time per

grid point per iteration is increased, the number of total iterations is substantially decreased; especially when the ξ-direction is aligned with the main flow direction. Of equal importance, this method also provides a substantial improvement in efficiency of data management of large 3-D data bases and is fully vectorized for fast vector processing, as we shall discuss in a later section.

Each of the flux difference vectors expressed in curvilinear coordinates is split according to the direction of the characteristic wave propagation by using the locally one dimensional analogy of the similarity transformation that diagonalizes the transformation matrix $\widetilde{A}$ of the flux difference vector ΔF by the conservative variables q, through the relations

$$\Delta F \equiv \widetilde{A}\Delta q \equiv \overline{MT}D\overline{T}^{-1}\widetilde{M}^{-1}\Delta q \tag{8}$$

where $\overline{M}$ is the transformation matrix of the primitive variable differences into the conservative variable differences,

$$\overline{M} = \begin{pmatrix} 1 & 0 & 0 & 0 & 0 \\ \overline{u} & 1 & 0 & 0 & 0 \\ \overline{v} & 0 & 1 & 0 & 0 \\ \overline{w} & 0 & 0 & 1 & 0 \\ \dfrac{\overline{u^2+v^2+w^2}}{2} & \overline{u} & \overline{v} & \overline{w} & 1 \end{pmatrix}$$

and $\overline{T}^{-1}$ is the transformation matrix of the primitive variable differences into the characteristic variable differences,

$$\overline{T}^{-1} = \begin{pmatrix} \dfrac{-1}{\overline{\rho}} & 0 & 0 & 0 & \dfrac{1}{\overline{\overline{\gamma P}}} \\ 0 & \overline{x_\eta}' & \overline{y_\eta}' & \overline{z_\eta}' & 0 \\ 0 & \overline{x_\psi}' & \overline{y_\psi}' & \overline{z_\psi}' & 0 \\ 0 & \dfrac{\overline{\tilde{\xi}}'_x}{\overline{\rho c}} & \dfrac{\overline{\tilde{\xi}}'_y}{\overline{\rho c}} & \dfrac{\overline{\tilde{\xi}}'_z}{\overline{\rho c}} & \dfrac{1}{\overline{\overline{\gamma P}}} \\ 0 & \dfrac{-\overline{\tilde{\xi}}'_x}{\overline{\rho c}} & \dfrac{-\overline{\tilde{\xi}}'_y}{\overline{\rho c}} & \dfrac{-\overline{\tilde{\xi}}'_z}{\overline{\rho c}} & \dfrac{1}{\overline{\overline{\gamma P}}} \end{pmatrix}$$

where the upper prime denotes

$$\overline{x_\eta}' = \overline{x_\eta}/\sqrt{\overline{x_\eta}^2 + \overline{y_\eta}^2 + \overline{z_\eta}^2},$$

$$\overline{\tilde{\xi}}'_x = \overline{\tilde{\xi}}_x/\sqrt{\overline{\tilde{\xi}}_x^2 + \overline{\tilde{\xi}}_y^2 + \overline{\tilde{\xi}}_z^2}\ ;$$

similarly, in all the other variables. The volumetric internal energy $P \equiv p/(\gamma - 1)$ is a primitive variable of the formulation.

D is a unit matrix which is split into three complementary D^+, D^-, and D^0 diagonal matrices. The diagonal coefficients of these matrices are 0's and/or 1's according to the propagation direction of the characteristic waves, as given by the sign of the eigenvalues of the transformation matrix $\widetilde{A}$. Thus D^+ has 1's only on the diagonal coefficients of the rows corresponding to the rows of $\widetilde{A}$ with positive eigenvalues; D^- has 1's only on the diagonal coefficients corresponding to negative eigenvalues, while D^0 is the complementary matrix. This matrix D^0 which is not present in other numerical methods provides increased robustness and stability. The eigenvalues for the fluxes, e.g. in the ξ-direction are

$$\overline{\overline{W}}^{\xi} \quad , \quad \overline{\overline{W}}^{\xi} + \overline{\overline{\xi}}\overline{c} \quad , \quad \overline{\overline{W}}^{\xi} - \overline{\overline{\xi}}\overline{c} \quad , \text{where} \tag{9}$$

$$\overline{\overline{W}}^{\xi} = (\overline{\overline{\xi}}_x\overline{\rho u} + \overline{\overline{\xi}}_y\overline{\rho v} + \overline{\overline{\xi}}_z\overline{\rho w})/\overline{\rho} \tag{10}$$

is the component of the contravariant averaged velocity,

$$\overline{\overline{\xi}} = (\overline{\overline{\xi}}_x^2 + \overline{\overline{\xi}}_y^2 + \overline{\overline{\xi}}_z^{\,2})^{1/2} \quad , \text{and} \tag{11}$$

$$\overline{c} = \overline{\gamma p}/\overline{\rho} \quad \text{is the average sound speed.} \tag{12}$$

Consequently, the flux difference vector of equation (8) is split as

$$\Delta F \equiv \nabla F^+ + \Delta F^- \equiv (\widetilde{A}^+\nabla + \widetilde{A}^-\Delta)q \tag{13}$$

where

$$\widetilde{A}^{\pm} = \overline{MT}D^{\pm}\overline{T}^{-1}\widetilde{M}^{-1} \tag{14a}$$

and

$$\widetilde{A}^0 = \overline{MT}D^0\overline{T}^{-1}\overline{M}^{-1} \tag{14b}$$

∇ is the backward-difference operator, Δ is the forward-difference operator.

By analogy to the well known result for the scalar advection equation, unconditionally stable Euler implicit methods are constructed of the flux difference split pieces by upwind (forward) differencing pieces associated with negative eigenvalues and, similarly, backward differencing pieces with positive eigenvalues. The method is well-posed in the case that the magnitude of any eigenvalue is zero; in these cases, the internal approximation which effectively asserts that the characteristic quantity associated with a zero advective eigenvalue doesn't change[14], added to the system of matrix equations only on the left hand-side makes the system to be stable and produces smooth solutions.

3-D DDADI Implicit Diagonal Dominant Factorization

Multi-dimensional linearized block implicit schemes employ approximate factorization of the left-hand side matrices to permit solving coupled matrix equations in one family of coordinates at a time; otherwise, the solution of the system of equations would not be practical under current computers. Different from the relaxation scheme of the CSCM method[5], most well known relaxation methods[15,16,17] have relied upon less accurate techniques of approximate factorizations that are not linearly unconditionally stable[18] in three dimensions and less robust in two.

The 3-D diagonal-dominant approximate factorization DDADI[5] of the unfactored implicit upwind matrix equations is used to solve the system of equations. The matrices corresponding to zero eigenvalue and that are added to I on the left hand side is shown in the relationships described below. Then, the 3-D DDADI system is represented as:

$$(I + L)\delta q = -Lq \tag{15}$$

where the operator L is defined as

$$L = L_\xi + L_\eta + L_\psi \tag{16}$$

and

$$L_\xi = \widetilde{A}^+_\xi \nabla_\xi + \widetilde{A}^-_\xi \Delta_\xi + \widetilde{A}^0_\xi \tag{17a}$$

$$L_\eta = \widetilde{A}^+_\eta \nabla_\eta + \widetilde{A}^-_\eta \Delta_\eta + \widetilde{A}^0_\eta \tag{17b}$$

$$L_\psi = \widetilde{A}^+_\psi \nabla_\psi + \widetilde{A}^-_\psi \Delta_\psi + \widetilde{A}^0_\psi \tag{17c}$$

The diagonal dominant relaxation scheme for the method of planes is written as:

$$(I + A_\xi + L_\eta + L_\psi)\delta q = -L^{n,n+1} q \tag{18}$$

where the absolute value matrix operator A_ξ on the diagonal is defined as

$$A_\xi = \widetilde{A}^+_\xi - \widetilde{A}^-_\xi + \widetilde{A}^0_\xi \tag{19}$$

and the off-diagonal matrix operator $L_\xi - A_\xi$ is only effectively included in the right-hand-side of equation (18). Equation (18) is solved on each plane in the forward and backward space marching sweeps on alternating time steps, and the matrix operator $L^{n,n+1}$ indicates that the data belonging to all previously computed planes are already updated.

In solving equation (18), the diagonally dominant approximate factorization of the left-hand-side of equation (18) in the other two directions leads to the following block tridiagonal equation sequence:

$$(D + L_\eta - A_\eta)\delta q^* = -L^{n,n+1} q \tag{20}$$

$$(D + L_\psi - A_\psi)\delta q = -D\delta q^* \tag{21}$$

with

$$q^{n+1} = q^n + \delta q^n \tag{22}$$

and where the diagonal matrix operator D is defined as

$$D = I + A_\xi + A_\eta + A_\psi \tag{23}$$

Observe that the absolute values of the eigenvalues for all coordinate directions are in the diagonally dominant matrix D, equations (20) and (21).

The Newton-Raphson inner iteration is applied by setting up the equations, solving and updating the base data at each plane twice during the forward and backward sweep procedure. This inner iteration is central to the improvement in fast rate of convergence of the solution of the nonlinear system of equations. The nonlinearities of the Navier-Stokes equations are better approximated in the updated locally active matrices, and the characteristic waves are propagated more accurately[6,14].

Boundary Conditions

Implicit characteristic boundary procedures based on the approach of reference 5 are applied at each boundary where at least one characteristic wave propagates from the boundary toward the interior of the computational domain. The boundary approximations are added as system of equations similar to the one for interior grid points of equations (18); except for the absence of convection matrices $\widetilde{A}^+$ at left boundaries and $\widetilde{A}^-$ at right boundaries which are replaced by local transformation matrices that contain the linear representations of the characteristic variables and auxiliary (imposed) boundary conditions in terms of conservative variables.

For supersonic freestream inflow conditions such as the outer boundary of reentry vehicles, the conservative flow variables are properly frozen. For supersonic outflow conditions, the conservative variables are properly extrapolated from the interior domain. For subsonic outflow, such as the one inside of the boundary layer zone, no change in the static pressure is imposed by the solution procedure at the outflow boundary, however, the solution procedure is also applied differencing along the outflow boundary. For viscous wall boundaries, no-slip conditions are applied and/or specified blowing/suction mass rates, together with specified wall temperature and/or adiabatic wall conditions. At symmetry planes, implicit symmetric approximations of the flux contributions beyond the boundary are imposed by symmetry relations based on the interior procedure toward the boundary.

Data Storage

Three-dimensional numerical simulations usually employ large storage capacity of the order of few to several million words of storage. For example, the simulation[19] of the 3-D flow over a conical afterbody containing a centered propulsive jet used about five million words of data base with twenty-three variables per grid point. Due to the single data level relaxation technique and with recomputed metrics, our method requires only eight variables per grid point, corresponding to the three coordinate directions and the five dependent variables. For large data bases on the CRAY-XMP computer, these variables are stored in SSD solid-state devices. These devices have a fast transfer rate to the central memory of the vector processors where our method operates on only a few (five for the second order method) ξ data planes at a time. Without the single level technique, at least five other (residual) variables with total grid dimensions will be required. Other variables may also be stored in order to decrease the running time in the processor and avoid repetitive and unnecessary computation, particularly the nine metric coefficients and one Jacobian of the coordinate transformation.

Data Management

With first order differencing in the ξ-direction, such as is implemented at present, the ξ sweeps require loading the data of planes $J-1$, J, and $J+1$ into central memory in order to process the data of plane J. In coding, the computation of the flux terms and matrix coefficients are fully vectorized in the ξ plane. The boundary conditions and solvers are also vectorized. Once the data of plane J is updated, this new data is stored, and the data of plane $J+2$ (on a forward sweep) is loaded into central memory in order to advance the data of plane $J+1$. Thus, the complete forward ξ sweep requires only loading data base once into central memory, and so does the backward ξ sweep.

The Beam and Warming[15] approximate factorization conceptually requires loading the data base into central memory at least three times, once in every coordinate direction. The main problem is that large data bases (that

exceed core) cannot be loaded in entirety into central memory; thus the data base must be loaded fractionally in line arrays or group of line arrays aligned in the processing direction. However, if the data base has been stored aligned in one coordinate direction, the loading of the line or group of lines data aligned into another coordinate directions require the transposition of the data base.

To facilitate the transposition the "pencil" system developed by Lomax and Pulliam[20] stores the data base in small cubes, as resembling a Rubik cube. Group of line arrays are loaded into central memory as a "pencil" by transferring the data of adjacent cubes aligned in the processing direction. This method still requires two or more additional total transfer of data into central memory per iteration[19] than our single level method.

Initial Conditions

The initialization of the three-dimensional data is very significant in order to obtain convergence in comparatively comparatively few numerical iterations. In this case, solutions are first obtained for the case of 3-D axisymmetric flow with the 2-D code for axisymmetric flows[5,21]. This kind of solutions are obtained within a few hundred iterations with about 9 10^{-5} cpu seconds per iteration and per grid point. This is a reasonable fast processing time considering that this is DDADI diagonal-dominant approximate factorization scheme. Then the solution is run with the 3-D code, changing only the free stream flowfield conditions, and the solution is obtained within N complete alternating sweeps where N is about half of the grid points in the streamwise direction. The three dimensional solutions relaxed in about 60 global iterations and about an hour of CPU time. Simpler initialization procedures can be similarly effective.

Numerical Results

Numerical results of the hypersonic flow around a reentry vehicle (RV) are now presented. The geometry of the vehicle is a sphere-cone-cylinder-flare body. This geometry has previously been treated as Case 4 of Kim and Lewis[9]. Each part of the cone, cylinder, and flare section was 10 nose-radii axial lenght with a half angle of 16° in the cone surface and a half angle of 12° in the flare surface. The free stream Mach number is 22, the Reynolds number is 10^5, Prandtl number is 0.7, and the ratio of specific heats γ=1.4. A cold wall boundary condition was applied with $T_W/T_\infty = 7$.

Figures 1a and 1b show different views of the 64×31 body mesh surface of the 64×47×31 three dimensional mesh on the reentry vehicle. The computational mesh has 64 points in the streamwise direction, 47 points from the body wall toward the outer boundary, and 31 points in the circumferential direction. The mesh has been constructed by using efficient 2-D algebraic procedures[22] based on transfinite interpolation in the upper and lower azimuthal symmetry planes, shown in Figure 1c, and a similar procedure with rotation between these two planes in order to define the remaining grid planes, as is shown in Figure 1d. Figure 1d shows a projection normal to the axis of the body of the computational mesh plane in the middle of the flare section. This simple procedure is very effective for this regular geometry to define the grid with minimum distortions and gives an excellent resolution around the body geometry and corner singularities. The grid lines are normal to the body wall and follow the general geometry of the bow shock.

Firstly, Figures 2a, 2b, and 2c show contour plots of Mach number, normalized pressure, and density of the hypersonic axisymmetric flow with 0° of angle of attack along a streamwise plane. The pressure is normalized with its free stream value. The bow shock is well captured and the contour lines in the shock layer are smooth and free of oscillations and/or instabilities. The expansion waves generated at the cone-cylinder corner and the weak oblique compression shock generated in the cylinder-flare corner are well captured by the method as shown in the pressure contours. The non-alignment of the grid with the bow shock is reflected as some small changes in the shock distribution, as well as, in the lower resolution in the flare section. The use of adaptive grid techniques should produce optimal results in this kind of simulation.

In order to test the numerical results, we show in Figures 3a, 3b, and 3c similar contour plots to those of Figures 2, but obtained with the 2-D code for 3-D axisymmetric flows. The agreement is excellent between the flow contours of the 3-D and the axisymmetric 3-D simulations. The external bow shock, the expansion fan, and recompression shock are almost identical in both simulations. Minor differences can be seen in the leeward side of the cylinder-body section.

Figures 4a, 4b, and 4c show the contour plots of Mach number, normalized pressure, and density of the hypersonic flow at 10° of angle of attack along the bisymmetry plane. This numerical solution was obtained after running 60 global iterations or complete alternating sweeps over the axisymmetric solution. The residuals of the equation of motions decreased at least 3 orders of magnitude and the solution was converged. The flow structures are well captured and the contour lines are smooth and free of oscillations and/or instabilities. The expansion waves generated at the cone-cylinder corner and the weak oblique compression shock generated in the cylinder-flare corner are well captured by the method as shown in the pressure contours. Also evident is the inflection of the bow shock with the interaction of the expansion fans off the cone-cylinder junction. The pressure and density contours show a normal section of the recompresion shock off the cylinder-flare junction.

Figure 5a shows the projection of the surface body mesh onto the bisymmetry plane, while Figure 5b show the contour plot of the normalized pressure on this plane. The effect of the free stream angle of attack on the pressure distribution is clearly defined in this Figure 5b, the highest contour values are on the sphere surface in the windward side and the smallest contour values are on the cylinder section in the leeward side. Figure 6a shows the surface pressure coefficient versus distance along the body surface. The horizontal axis of this plot is centered on the intersection of the axis of symmetry of the RV with the surface of the sphere section. The symbols show the pressure coefficients at 10° angle of attack along the body surface at every 15° from the bisymmetry plane, while the solid line shows the pressure coefficient at 0° angle of attack. Figure 6b shows a section of Figure 6a of the pressure distribution along the sphere-body section. The effects of the free stream angle of attack is well captured. There is some lack of smoothness near the pole of the grid topology due to an inconsistency of the grid spacing with the cross pole difference scheme that does not solve at the pole. The pole should have been "buried" at half cell spacing in the mesh.

Figures 7 show normalized pressure contours of cross sectional mesh planes projected onto the normal plane to the axis of body symmetry. Figures 7a, 7b, and 7c correspond to midplane section of the cone, cylinder, and flare sections, respectively, at 10° of angle of attack. On the other hand, Figure 7d correspond to midplane section of the flare section at 0° of angle of attack. Similarly, Figures 8 show the density contours corrsponding to the respective Figures 7. These figures show the three-dimensionality of the flow structures, the development of the bow shock, the 3-D zone of expansion fan, and 3-D zone of recompression shock. The complexity of the flow is shown to be well captured by the CSCM3D numerical method.

Concluding Remarks

The 3-D CSCM compressible Navier-Stokes algorithm has been improved and extended to simulate external hypersonic flows at angle of attack. The method combines the best features of storage and processing efficiency of PNS space marching procedures with the generality of time dependent techniques to solve flows with elliptic and streamwise separated zones. The 3-D DDADI diagonal-dominant approximate factorization, together with well posed implicit boundary approximations, and the implicit upwind difference algorithm provide robust stability and fast relaxation of the method. Numerical results at 0deg and 10deg angle of attack of a sphere-cone-cylinder-flare reentry vehicle are presented. The numerical results are consistent with axisymmetric simulations and with previous experience in external hypersonic flows. The robustness and stability of the CSCM3D method, as well as, its fast convergence rate make this method very appropiated for simulations including chemical reactions and adaptive grid techniques.

Acknowledgements

The work was partially supported by NASA-Ames Research Center under contract NAS2-12243 and the Air Force Office of Scientific Research under contract F49620-85-C-0081.

References

1. Anderson, J.D.: "A Survey of Modern Research in Hypersonic Aerodynamics," AIAA-84-1578, June 1984.
2. Bardina, J., and Lombard, C.K.: "Three Dimensional CSCM Method for the Compressible Navier-Stokes Equations with Application to a Multi-Nozzle Exhaust Flowfield," AIAA-85-1193, July 1985.
3. Lombard, C.K. and Nagaraj, N.: "Extensions of the CSCM Upwind Methodology for Nonequilibrium Reacting Gas Flows," To be presented at the *International Symposium on Computational Fluid Dynamics-Sydney*, August 1987.
4. Lombard, C.K., Raiszadeh, Farhad and Bardina, Jorge: "Efficient, Vectorizable Upwind Implicit Relaxation Algorithm for Three-Dimensional Gasdynamics," Presented at the SIAM Spring Meeting, Pittsburgh, PA, June 1985.
5. Lombard, C.K., Bardina, J., Venkatapathy, E. and Oliger, J.: "Multi-Dimensional Formulation of CSCM - An Upwind Flux Difference Eigenvector Split Method for the Compressible Navier-Stokes Equations," AIAA-83-1895, July 1983.
6. Lombard, C.K., Bardina, J., and Venkatapathy, E.: "AOTV Bluff Body Flow - Relaxation Algorithm," published in *Thermal Design of Aeroassisted Orbital Transfer Vehicles,* ed. by H.F. Nelson, Vol. 96 of Progress in Astronautics and Aeronautics, 1985.
7. Lombard, C.K., Venkatapathy, E. and Bardina, J.: "Universal Single Level Implicit Algorithm for Gasdynamics," AIAA-84-1533, 1984.
8. Bardina, J., Venkatapathy, E., and Lombard, C.K.: " Two Dimensional and Axisymmetric Heat Transfer Results with the CSCM-S Upwind Implicit Algorithm," published in *Thermophysical Aspects of Re-entry Flows,* ed. by J.N. Moss and C.D. Scott, Vol. 103 of Progress in Astronautics and Aeronautics Series, AIAA, 1986.
9. Kim, M.D., and Lewis, C.H.: "Computation of Hypersonic Viscous Flow Past General Bodies at Angle of Attack and Yaw," AIAA-82-0225, January 1982.
10. Baldwin, B.S. and Lomax, H.: "Thin Layer Approximation and Algebraic Model for Separated Turbulent Flows," AIAA 73-257, 1973.
11. Bradshaw, P.: "Prediction of the Turbulent Near Wake of a Symmetric Airfoil," *AIAA J.*, Vol. 8, p.1507, 1970.
12. Lombard, C.K., Bardina, J., Venkatapathy, E., Yang, J.Y., Luh, R.C-C., Nagaraj, N., and Raiszadeh, F.: "Accurate, Efficient, and Productive Methodology for Solving Turbulent Viscous Flows in Complex Geometry," Tenth Intnl. Conf. on Numerical Methods in Fluid Dynamics, June 23-27, 1986.
13. Yang, J.Y., Lombard, C.K. and Bardina, J.: "Implicit TVD Schemes for the Euler Equations with Bidiagonal Approximate FActorization," *International Symposium on Computational Fluid Dynamics, Tokyo, Japan,* Vol. 1, pp. 239-250, 1985.
14. Lombard, C.K.: "Conservative Supra-Characteristics Method for Splitting the Hyperbolic Systems of Gasdynamics for Real and Perfect Gases," NASA CR-166307, 1982.
15. Beam, R.M. and Warming, R.F.: "An Implicit Factored Scheme for the Compressible Navier-Stokes Equations," *AIAA J.*, Vol. 16, No. 4, April 1978, pp. 393-402.
16. McDonald, H, and Briley, W.R.: "Three-Dimensional Supersonic Flow of a Viscous or Inviscid Flow," Journal of Computational Physics, Vol. 19, pp. 150-178, 1975.
17. Steger, J. L., and Warming, R. F.: "Flux Vector Splitting of the Inviscid Gasdynamic Equations with Application to Finite Difference Methods," NASA TM 78605.
18. Chakravarthy, S. R.: "Relaxation Methods for Unfactored Implicit Upwind Schemes," AIAA 84-0165, 1984.
19. Deiwert, G.S.: "Three-Dimensional Flow Over a Conical Afterbody Containing a Centered Propulsive Jet: A Numerical Simulation," AIAA 83-1709, 1983.
20. Lomax, H. and Pulliam, T.H.: "A Fully Implicit Factored Code for Computing Three-Dimensional Flows on the Illiac IV," *Parallel Computers,* G. Rodriguez, Ed., Academic Press, NY, 1982, pp. 217-250.
21. Bardina, J., Venkatapathy, E., Nystrom, G., and Lombard, C.K.: "CSCM Methodology for Cavity Flow Design in a Supersonic Wedge Flow," AIAA-87-0518, January 1987.
22. Luh, R. C-C., Nagaraj, N., and Lombard, C.K.: "Simplified Algebraic Grid Generation in Patched Mesh Systems," AIAA-87-0200, January 1987.

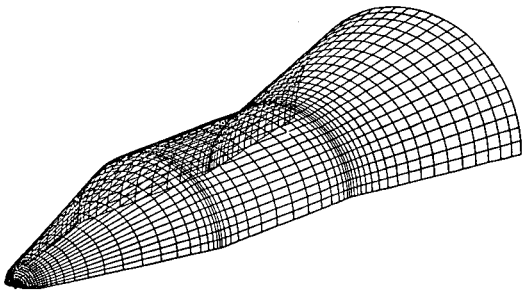

Figure 1a. 3-D view of surface mesh of sphere-cone-cylinder-flare reentry vehicle body.

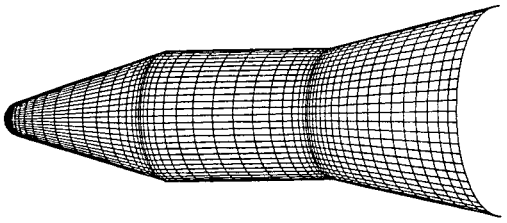

Figure 1b. 3-D view of surface RV mesh.

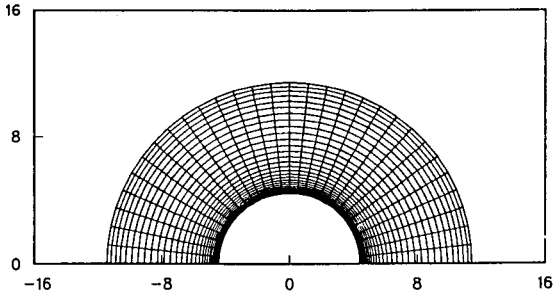

Figure 1d. Normal projection of cross sectional mesh in flare-body sector.

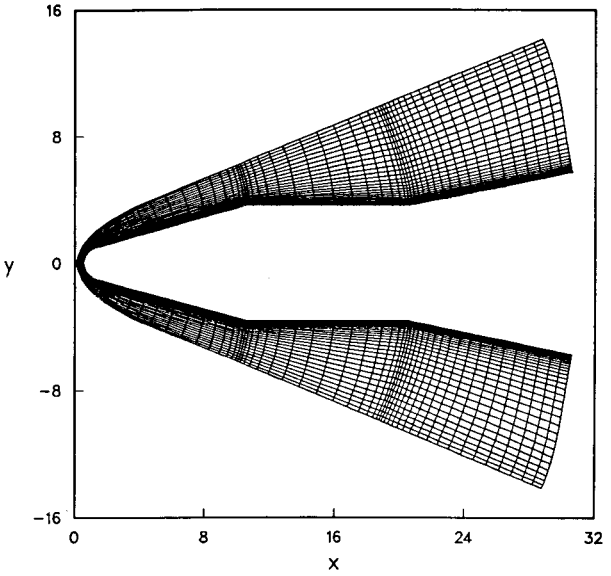

Figure 1c. Computational mesh on bisymmetry plane of RV vehicle.

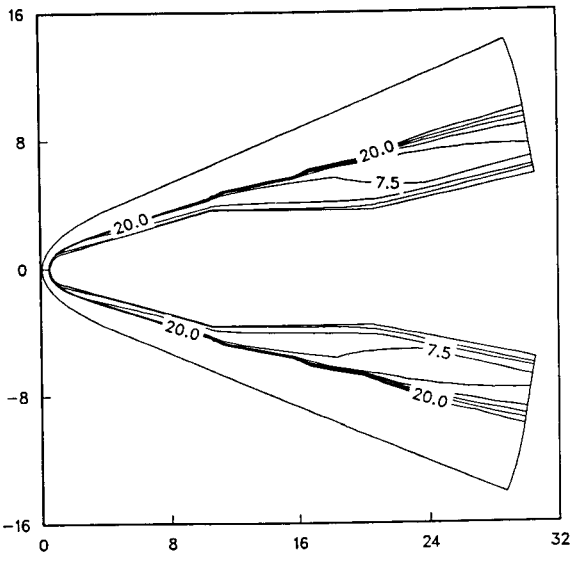

Figure 2a. Mach contour lines on bisymmetry plane. 3-D simulation of hypersonic axisymmetric flow.

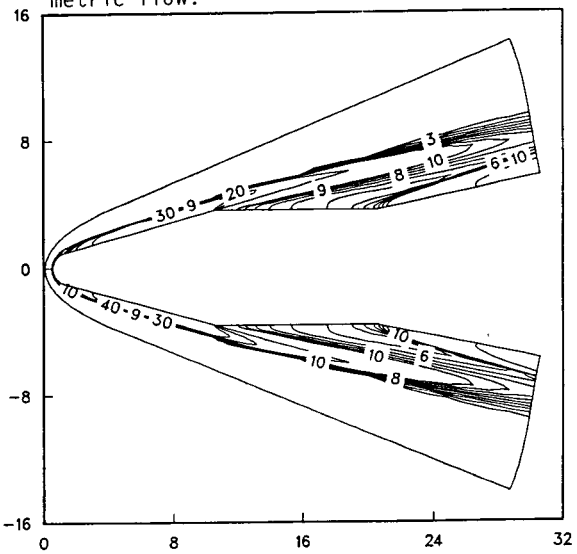

Figure 2b. Normalized pressure contour lines.

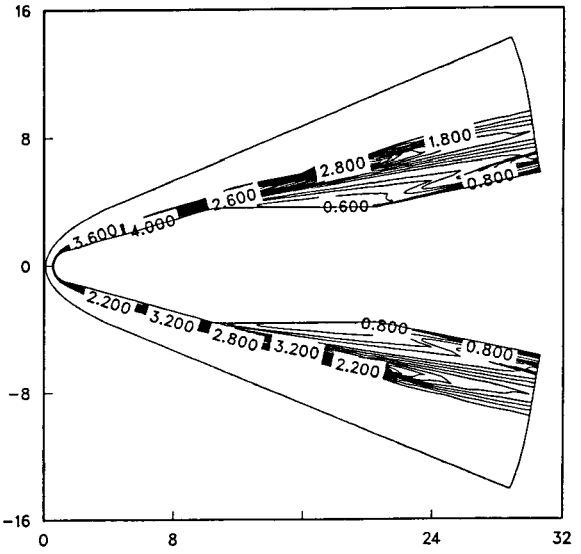

Figure 2c. Density contour lines.

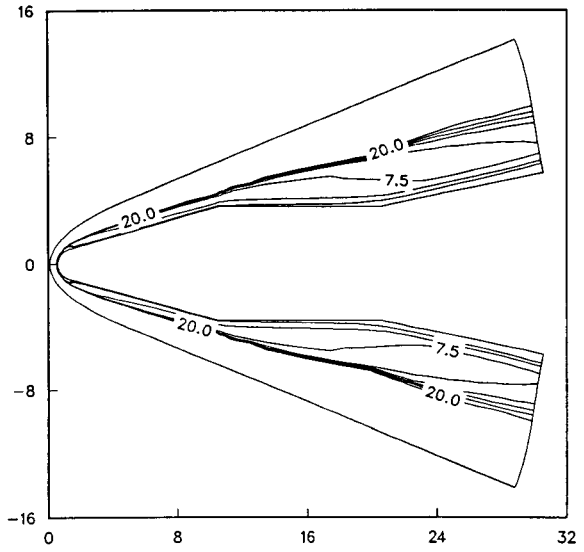

Figure 3a. Mach contour lines on bisymmetry plane. 2-D axisymmetric simulation.

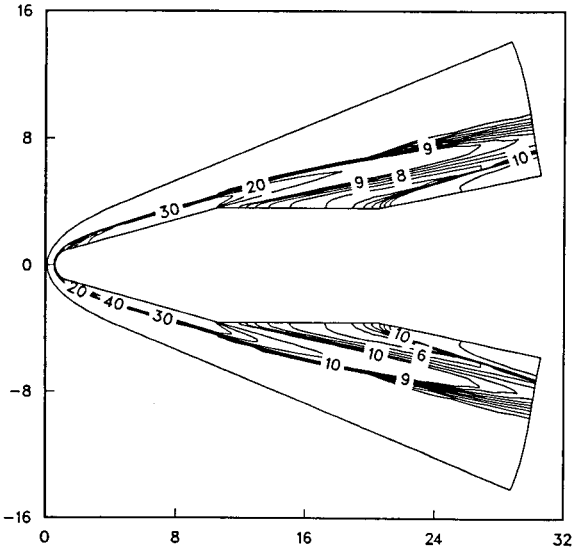

Figure 3b. Normalized pressure contour lines.

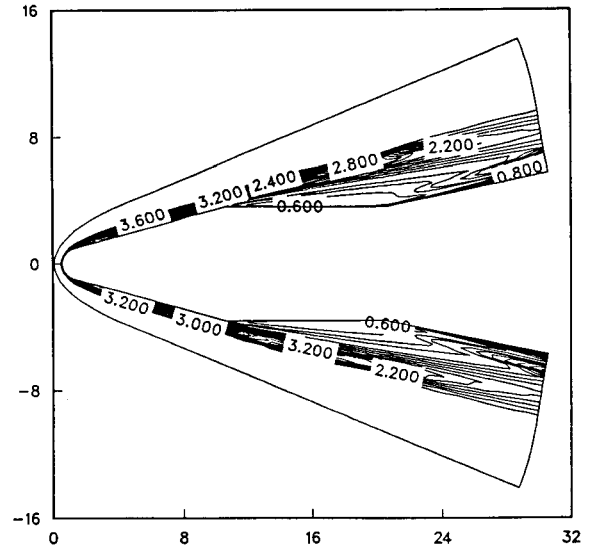

Figure 3c. Density contour lines.

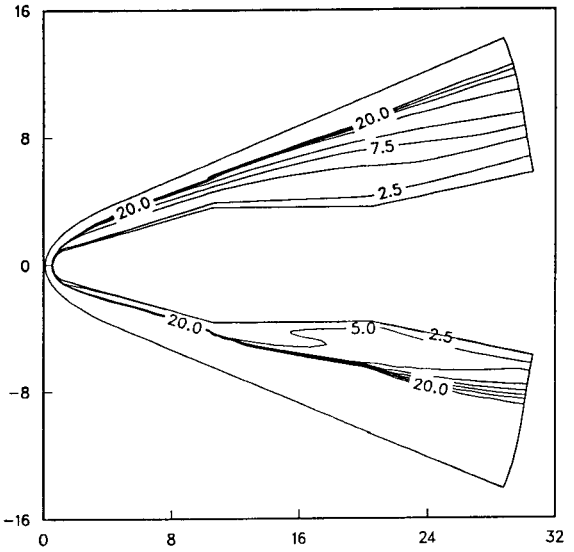

Figure 4a. Mach contour lines on bisymmetry plane. 3-D simulation of hypersonic flow at 10° angle of attack.

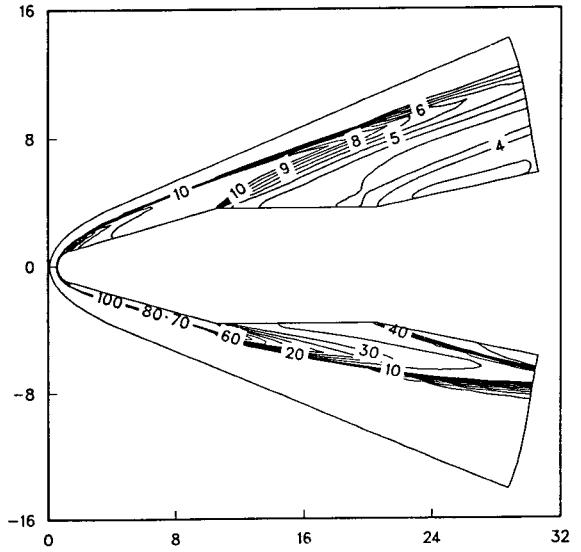

Figure 4b. Normalized pressure contour lines.

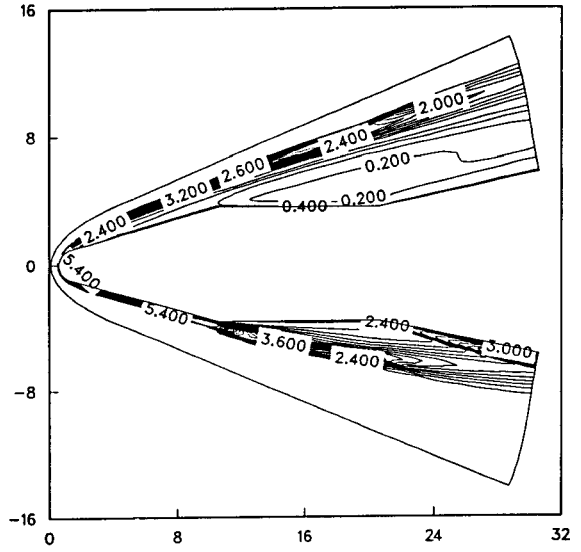

Figure 4c. Density contour lines.

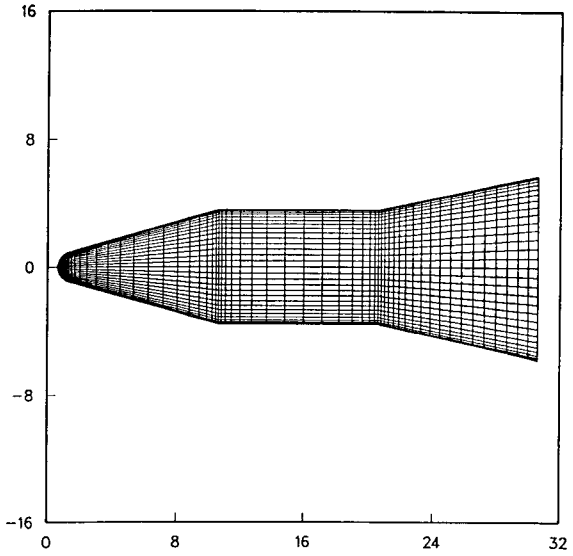

Figure 5a. Surface mesh body projected onto bisymmetry plane.

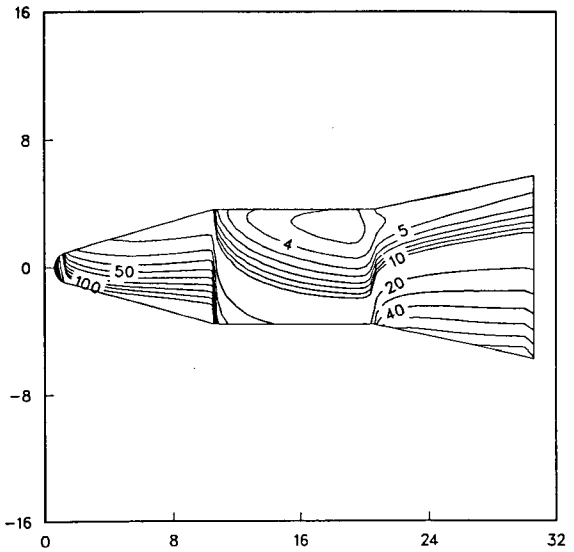

Figure 5b. Normalized pressure contour lines of hypersonic flow at 10° angle of attack corresponding to figure 5a.

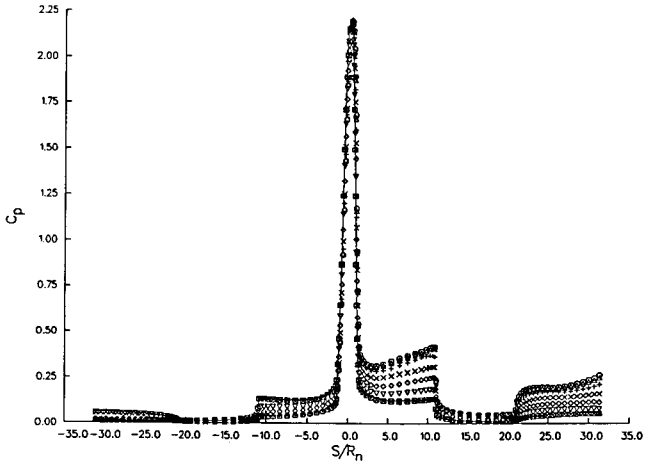

Figure 6a. Surface pressure coefficient along RV body. Symbols show predictions along planes at 0°,15°,30°,45°,60°,75°,and 90° off the bisymmetry plane of hypersonic flow at 10° angle of attack. Solid line shows prediction of axisymmetric flow at 0° angle of attack.

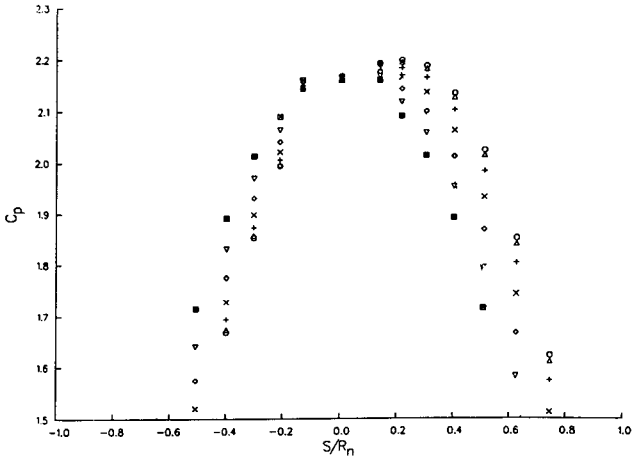

Figure 6b. Surface pressure coefficient along the sphere-body section. Symbols correspond to figure 6a.

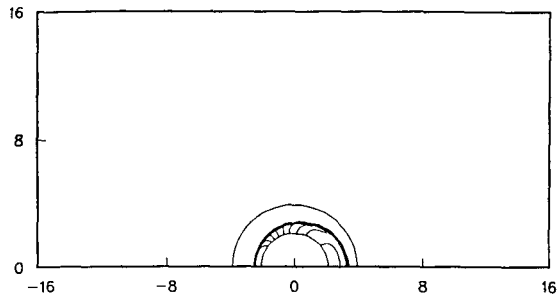

Figure 7a. Normalized pressure contour lines of hypersonic flow at 10° angle of attack, on cross sectional mesh midplane of cone-body section.

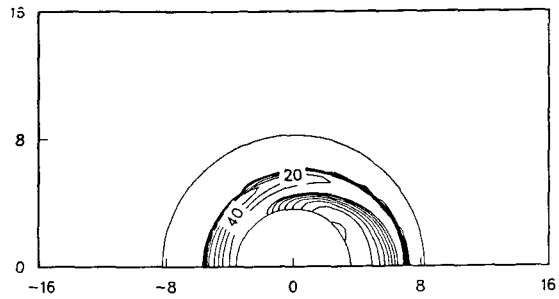

Figure 7b. Normalized pressure contour lines of hypersonic flow at 10° angle of attack, on cross sectional mesh midplane of cylinder-body section.

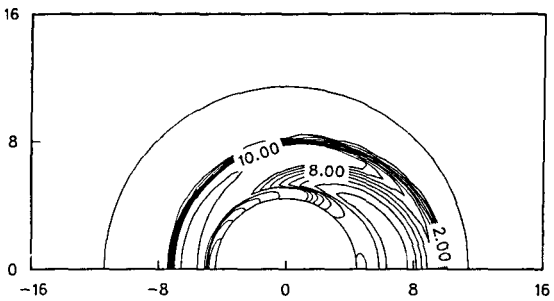

Figure 7c. Normalized pressure contour lines of hypersonic flow at 10° angle of attack, on cross sectional mesh midplane of flare-body section.

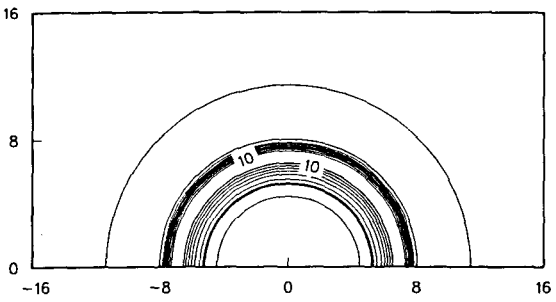

Figure 7d. Normalized pressure contour lines of axisymmetric hypersonic flow on cross sectional mesh midplane of flare-body section.

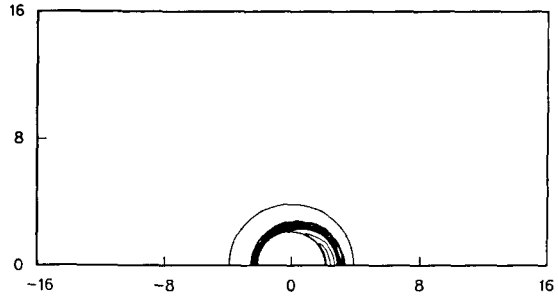

Figure 8a. Density contour lines, corresponding to figure 7a.

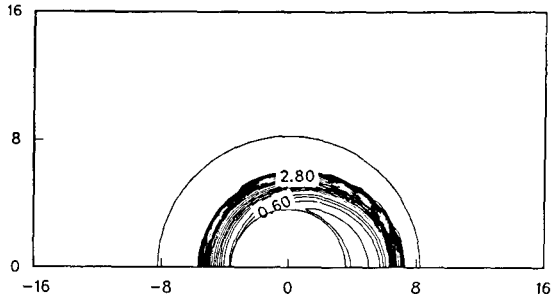

Figure 8b. Density contour lines, corresponding to figure 7b.

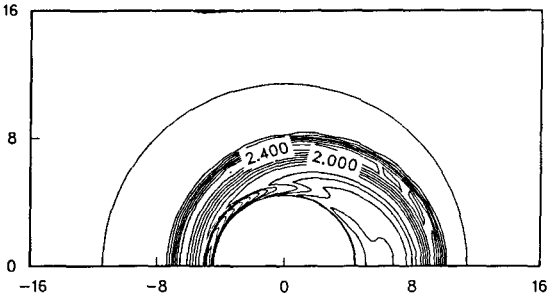

Figure 8c. Density contour lines, corresponding to figure 7c.

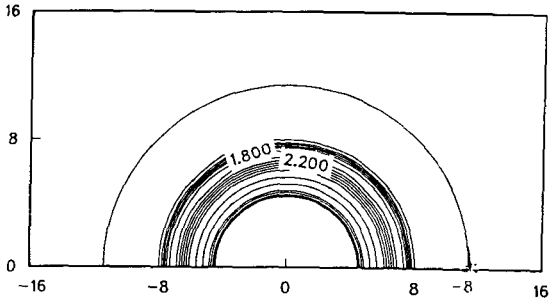

Figure 8d. Density contour lines, corresponding to the figure 7d.